Title: The mechanical effect of monitoring and controlling the impregnation in the resin infusion process

Juan-Antonio Almazán-Lázaro [1]*, Elías López-Alba [1] and Francisco-Alberto Díaz-Garrido [1]

[1] Department of Mechanical and Mining Engineering, Campus Las Lagunillas, University of Jaen, 23071 Jaén, Spain; elalba@ujaen.es; fdiaz@ujaen.es.

* Correspondence: jalmazan@ujaen.es; Tel.: +34-953212862

Abstract:

Nowadays, most of industries are optimizing their processes to make their products more competitive. In the composites manufacturing industry, there is a big gap between the almost fully automated processes and those which require an intensive labor-work. Although it has many advantages, the resin infusion (RI) process is characterized for its lack of automation. As a consequence, the results are strongly dependent on the process boundaries, the operator skills and expertise, and the result is usually far away from the optimum. In this work, the application of a novel methodology and its capability to maximize the mechanical properties of infusion-manufactured composite materials is presented. After manufacturing stitched and unstitched materials at different impregnation velocities, an optimum value was assessed. The application of this value during the manufacture has increased the tensile and impact properties.

Keywords: composite, control, mechanical properties, impact, tensile, voids.

1. Introduction

Nowadays, composite materials are becoming more popular in some sectors such as the automotive or sports due to their high specific mechanical properties. Weight saving is one of the most important goals for composite-based products and the light-weight manufacturing can reduce the costs [1] and weight up to 40% [2]. The higher mechanical performance of the material, the lower material amount is required. Then, achieving the maximum mechanical properties is a must to minimize the weight, the waste and optimize the resources. The process automation is a base to fulfill these objectives [3].

Most of composite manufacturing processes require a great effort of dry fiber handling and processing [4]. Many ideas have been proposed to deal with the challenge of its automation. Main efforts have been done in robotics, mainly to manage the dry fibers [5], [6] and automate the manufacturing of large parts [7]. Also, many experiences have also been focused on curing control [8]. Nevertheless, other stages of the process have not been deeply automated, such as the impregnation, also known as infiltration. Only limited literature is found in this area, specifically in the case of active control. In particular, Alms et al. [9] proposed a system to control the resin flow by modifying the mold external pressure and Sozer et al. [10] and Devillard et al. [11] analyzed the flow and corrected some undesirable disturbances in real time. As reviewed by Seyednouran [12], these techniques usually entail extensive and complex tooling. In this respect, this work tries to avoid these drawbacks by using a conventional mold and cost-effective methods.

Several manufacturing processes are available to produce continuous-fiber reinforced polymers, as reviewed by Rajak et al, [13]. LCM (liquid composited molding) techniques, such as RTM (resin transfer molding) and RFI (resin film infusion) or simply RI (resin infusion), are based on the impregnation of an initially dry fibers in the interior of a mold cavity. LCM techniques are widely used in the automotive and energy industries [4] as well as in some specific parts for aerospace applications [7]. Resin Infusion process is the preferred production method for large composite parts such as wind turbine blades, aircraft wing covers or boats. Nevertheless, RI processes show some reliability and repeatability challenges, mainly related with the impregnation quality and the intensive hand-work required. RTM uses a double-side rigid mold, and positive pressure is applied to force the resin to flow through the fibers, before reaching the vent port at the atmospheric pressure. In RI, one mold side is replaced by a flexible and airtight bag, and the applied differential pressure at the mold ports is generated only by a vacuum pump. The vacuum pump is plugged into one port, while the other port is connected to a resin pot at atmospheric pressure. It induces a flow movement and the impregnation through the defined path from the pot port(s) to the vacuum port(s) is performed. As the flow goes further, the pressure gradient is getting lower, as the applied pressure keeps constant and the impregnated length is increasing. Consequently, the impregnation velocity (i.e. flow front velocity) is getting lower as the flow front goes further. It can be modelled by the Darcy's model for porous media [14], as shown in Eq. 1~~Eq. 1~~ for the unidimensional case, where u is the flow front velocity, ΔP is the applied differential pressure, Δx is the impregnated distance, K is the unidimensional permeability factor, μ is the dynamic viscosity and $\emptyset$ is the porosity.

$$u = \frac{\Delta P \cdot K}{\Delta x \cdot \mu \cdot \emptyset} \qquad \text{Eq. 1}$$

Eq. 1~~Eq. 1~~, which is dependent of the flow position, can be rewritten as a function of the process time, Δt (Eq. 2~~Eq. 2~~).

$$u = \sqrt{\frac{\Delta P \cdot K}{\Delta t \cdot \mu \cdot \emptyset}} \qquad \text{Eq. 2}$$

As a consequence of the pressure gradient variation, while the rest of parameters in Eq. 1~~Eq. 1~~ and Eq. 2~~Eq. 2~~ are presumably constant, the velocity u is proportional to Δx^{-1} or $\Delta t^{-1/2}$. It means that very high velocities are induced at the beginning of the impregnation process, while low velocities can be expected at the end of the impregnation process. As a result, a non-homogeneous velocity pattern is produced in the laminate, which has negative effect in the material performance. The variation in the impregnation velocity has been reported as one of the main factors which generate internal defects in the final material [15]. This non-homogeneous velocity may change the impregnation performance and the defects generation phenomena, especially in dual-scale laminates, as it has been often reported [16]. Structurally, dry fiber reinforcements are usually arranged as dual-scale preforms, where empty spaces can be found at different locations. Micro-gaps are located among individual fibers, as macro-gaps are located among individual yarns. When the resin is forced to flow within the fibers and yarns, two phenomena drive the process. On the one hand, the applied external pressure induces a macro-flow going through macro-gaps as the lowest pressure losses are found there. This macro-flow is dominated by the viscous forces. On the other hand, due to the small scale of the micro-gaps, a noticeable capillary effect is also induced [17]. During the impregnation process, if one of these two flows is going faster than the another, the slowest one will has no time to fill their gaps completely. Consequently, voids are generated. When capillary phenomenon is dominating the impregnation, macrovoids are generated within the yarns. Otherwise, when the macro-flow is the fastest one, microvoids are generated within the individual fibers. Then, there is an intermediate value for the flow rate which minimizes both undesired phenomena [18] and the minimum void content will be obtained, as described by the V-shape curve in the work of Causse et al [19].

Many works have reported the negative effect of voids over the mechanical performance of composites for in-plane and out-of-plane loads [16], [20]. Specifically, authors such as

Leclerc et al. [21] and Olivero et al. [22] show reductions in the in-plane tensile properties when the void content is increased. Similarly, Patou et al. [23] reported a reduction in the out-of-plane impact properties as a consequence of voids presence. Also, the absorbed energy (i.e. damage) during the impact was higher in case of higher void content, as reviewed by Mehdikhani et al. [16]. In RTM, optimum velocity and pressure which maximize the mechanical properties were found [21], [24]. No related works are available in the literature for RI processes. In this study, low-velocity impact and tensile test have been chosen as representative tests to cover both in-plane and out-of-plane loads.

In this context, the initially proposed idea of Trochu et al. [25] of keeping the flow front velocity close to the optimal conditions in RTM is interesting, although it shows some uncovered challenges. As described by Causse et al, [19] and Leclerc and Ruiz [21], imposing a flow profile requires from the fiber/resin system characterization. Even when this characterization is done for each specific laminate, the application is not simple, especially in RI, where the flow rate is depending on the pressure throughout many variables. For complex geometries, corrections were successfully carried out by Causse et al. [19] in RTM, where the flow rate can be easily controlled. For RI, it implies an additional complexity in the setup, since the relationship between the velocity and the applied pressure gradient should be also characterized. Among the very limited literature, recently, He et al. [26] have used a real-time flow control system to minimize the void content in LCM processes, and noticeable improvements were reported.

To control the flow front velocity, the flow position should be firstly accurately measured. Some techniques have been proposed in the literature to track the flow front position. Di Fratta et al. [27] and Endruweit et al., [28] used pressure sensors embedded in the mold, although no further control was done. Optic fiber sensors were used by Ahn and Lee [29], as well as ultrasound sensors and resistive sensors, used by He et al. [26]. Most of these techniques are usually used as a single point methods and the reported information could be limited. Optical methods have also been used during the impregnation or permeability measurements, as reviewed by Grössing and coworkers [30] and recently for Geng et al. [31]. Nevertheless, as reported by Vernet et al., [32], the image processing is not applied at real time and subsequent image analysis is performed afterwards. Major difficulties in the flow controlling can be observed when complex laminates are impregnated. As permeability manages the flow behaviour, according to the Darcy's model, laminates with non-homogeneous fibre distribution or reinforcements could make the flow control more difficult [33]. In this respect, stitching, as a three-dimensional reinforcement [34], changes the flow behaviour, the defects generation and flow distribution could be unpredictable [35]. In this context, computerized vision, as a full field technique, allows to monitor the whole flow front in real time, whatever geometry or laminate is used.

Then, a novel cost-effective approach is proposed in this work for RI applications. It is based on a real time controller that is continuously monitoring and controlling the instantaneous flow front velocity according to the pre-defined optimum velocity goal. It allows keeping a constant and optimum flow front velocity during the whole impregnation process. The main advantage of this system is that the permeability distribution and the flow behaviour could remain unknown during the process, although the process is done at optimum values.

2. Experimental

To optimize the mechanical properties of RI manufactured composites, a novel manufacturing control approach is presented. Based on the relationship between the impregnation velocity and the mechanical properties, the flow front velocity is measured and controlled using a developed computer vision system.

2.1. Measuring and controlling the impregnation

As described by Eq. 1~~Eq. 1~~ and Eq. 2~~Eq. 2~~, the applied pressure should be modified continuously as a function of the time, t, or the flow position, Δx, to keep the velocity constant at optimum value. The proposed method to perform this work is schematically presented in the Figure 1~~Figure 1~~. In the first stage, the unknown material should be characterized. Mechanical tests are carried out for materials manufactured at different impregnation velocities in simple geometries. Optimum velocity can be assessed from these analyses. To manufacture materials with optimum properties, this previously calculated optimum velocity is given as an input in the algorithm. The algorithm reads the camera images, which is continuously taking pictures of the laminate. Using computer vision techniques, these images are processed in real time to detect the flow position and then, the instantaneous velocity can be calculated taking into account the processing framerate. The actual velocity is compared with the optimum velocity and then, the difference (i.e. error) is calculated. A proportional output signal is given to the adjustable valve as input. This valve manages the flowrate going inside the mold. Only in the case that the actual velocity is equal to the optimum, the valve position does not change. Otherwise, the valve is opened or closed as per the algorithm's output.

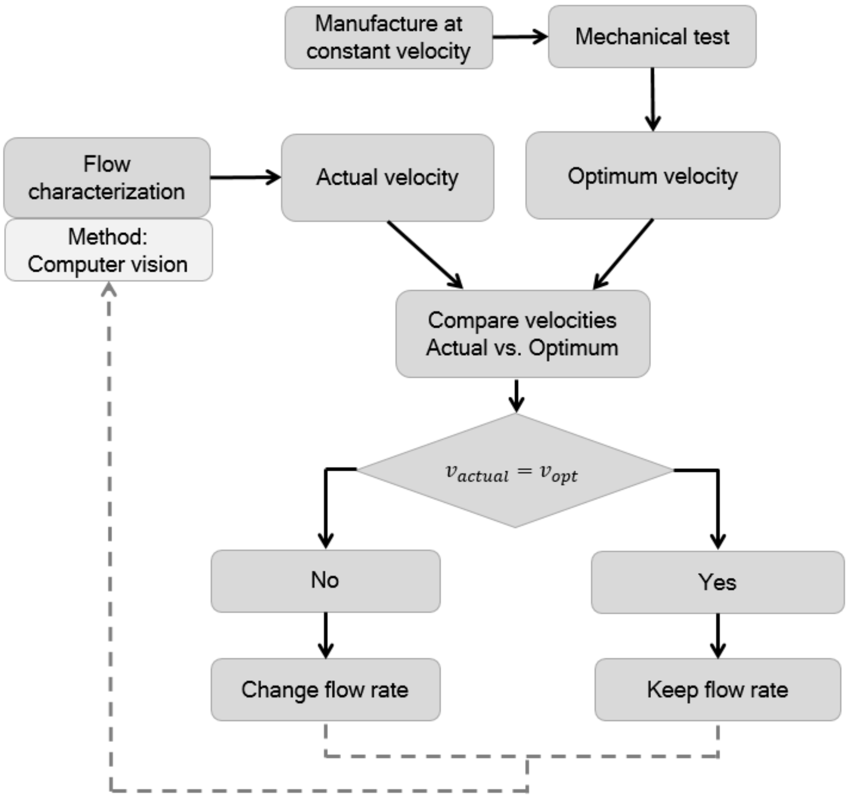

Figure 1. Flowchart of the adopted methodology.

The setup of this concept is shown in Figure 2Figure 2a. Once the mold is properly sealed after dry fiber placement, one port is connected to the resin pot. The other port is connected to the controlled valve, which is subsequently connected to the vacuum pump. A camera is located at the top of the mold to record the flow front during the impregnation process. The camera is continuously taking images of the laminate and they are processed in a computer in real time (Figure 2Figure 2b). Depending on the actual flow velocity, the valve is accordingly adjusted, after comparing the value with the optimum. The system is surrounded by an opaque box to avoid the influence of any external light, as it increases the robustness of the process. To process the images, an initial picture is taken before starting the process, which is set as the reference image. Then, when the process starts, images are taken at 10 frames per second and the reference image is subtracted pixel by pixel. As a result, the impregnated and unimpregnated area are clearly highlighted. Then, it is analyzed using computer vision techniques. Gradient-based operators are used to isolate the flow front at each taken picture. Once the flow front position is known, the velocity can be evaluated when consecutive images are analyzed. This instantaneous velocity is compared with the optimum value which was preliminary set in the controller for the specific material. According to the difference, the signal is proportionally applied on the valve to modify the resin flow rate to keep it in the optimum value.

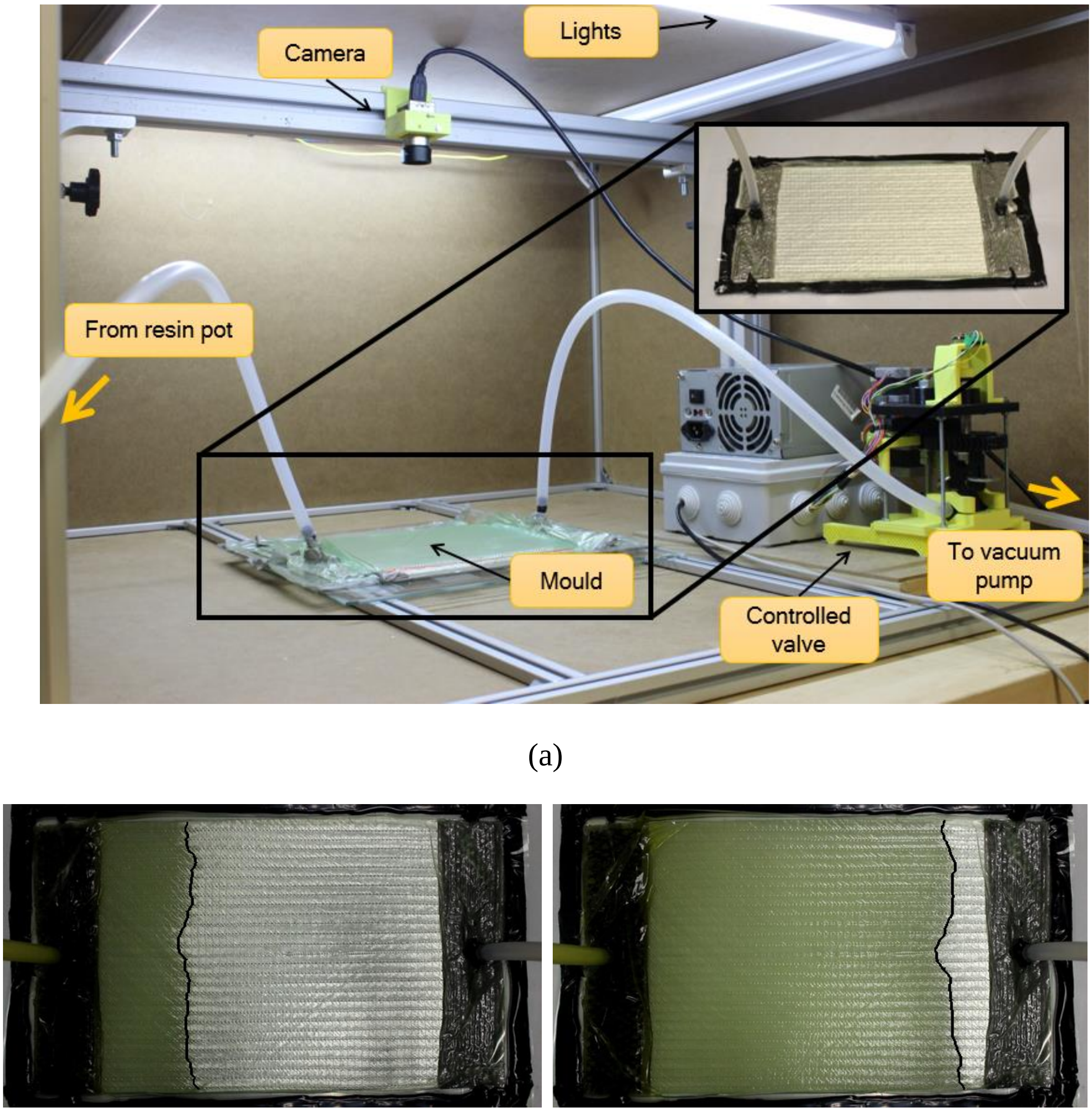

(a)

(b)

Figure 2. (a) Setup to impregnate the fabrics using a real-time velocity controller, and (b) example of camera pictures of flow front at two different times.

2.2. Equipment and materials

In addition to the previously introduced controlling system, other equipment and materials have been used to manufacture and test the specimens. A 900x700x2 mm^3 steel plate was used as a mold to manufacture all plate-shaped specimens. A wood box of 900x900x500 mm^3 has been used to isolate the setup from the external light conditions. As a matrix, a polyester-based system P4 TV-28 (DSM, Germany) has been used and catalyzed with M312 (Curox, Germany) at 2% weight. As a reinforcement, unidirectional 600g/m^2 E-glass fiber plies were used. To build the airtight bag, a 75 µm BF-32 (Airtech Inc, US) nylon bag was sealed using AT200Y tape (Airtech Inc, US). Vacuum was applied with an Edwards 80 pump (Edwards

Vacuum, UK). Stitching was performed using a Pffaf 3574 sewing machine with computer numerical control (CNC), available in the Leibniz Institute for Composite Materials, (Kaiserslautern, Germany) and Saba C50 thread (Amann & Sohne GmbH, Germany) was used. To measure the flow front position during the impregnation, a monochrome Mako 130B camera (Allied Vision, Germany) was used.

Finally, to perform the mechanical tensile test, a MTS 370.02 (MTS Systems Corporation, US) servohydraulic machine has been used. For impact tests, two drop towers have been employed. One, with 15 m height, is available in the Leibniz Institute for Composite Materials, (Kaiserslautern, Germany) while the another with 2 m is set at the University of Jaén (Spain). A hemispherical Ø16 mm impactor was set in both devices. Impactor position was continuously monitored using Digital Image Correlation. A high-speed camera was used to capture the images of the impact event. After that, a commercial solution (VIC-2D, Correlated Solutions, Irmo, SC, USA) was used to track the speckle pattern and calculate the position and the velocity during the impact. To analyze the damage of the impacted specimens, a backlight system has been used, as the change in the light transmission trough the thickness highlights the affected area, as other studies have reported [36].

2.3. Manufacturing and testing

To analyze the effect of controlling the impregnation velocity, different laminates were manufactured and tested under tensile and low-velocity impact tests. Tensile specimens were manufactured at different fibre orientation, as shown in Figure 3, where the arrow means the load application in tensile test. The orientation was changed by modifying the relative angle between the flow direction and the fiber orientation. Consequently, specimens were also cut perpendicularly to the flow front, aiming to minimize the flow variations along the size of the specimens. Three specimens were cut from each laminate and five laminates were manufactured at each orientation. For impact laminates, the target velocities were set constant for each laminate: 2.5 mm/s, 4.0 mm/s, 6.0 mm/s and 11.0 mm/s for unstitched laminates. For stitched laminates, slightly higher values were set, as they show higher permeabilities. Five specimens were manufactured at each velocity. Stitching was performed using a grid with 3.33 mm between stitches and 10 mm between seams in a squared distribution. One-side lock-stitch configuration was adopted.

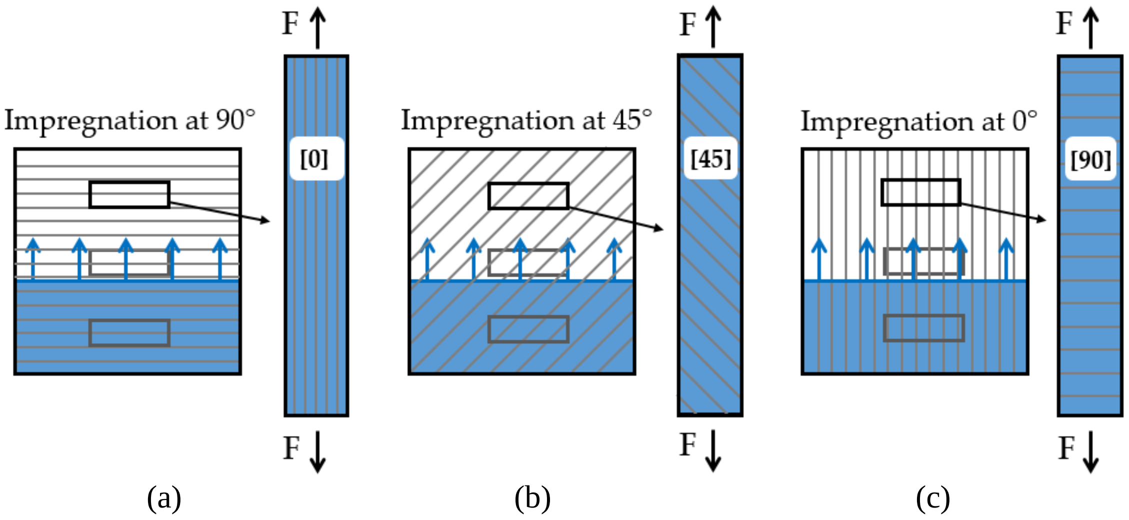

Figure 3. Specimens impregnation for tensile tests.

Subsequently, mechanical tests were performed. Firstly, tensile tests were carried out according to ASTM D3039 [37]. Optimum flow front velocity was calculated from these results, and the impregnation and tests were repeated using this value. Then, impact tests were performed according to ASTM D7136/7136M [38] using 13 J of impact energy, and then, 26 J was applied over the same specimens. The setup for the impact tests is shown in Figure 4, where the specimen's center was perpendicular and vertically aligned with the impactor axis. Digital image correlation technique (DIC) was used to measure the actual impactor velocity and displacement during the event, so speckle was added to the mobile frame. As a consequence of the high frame rate, an extra power light was required.

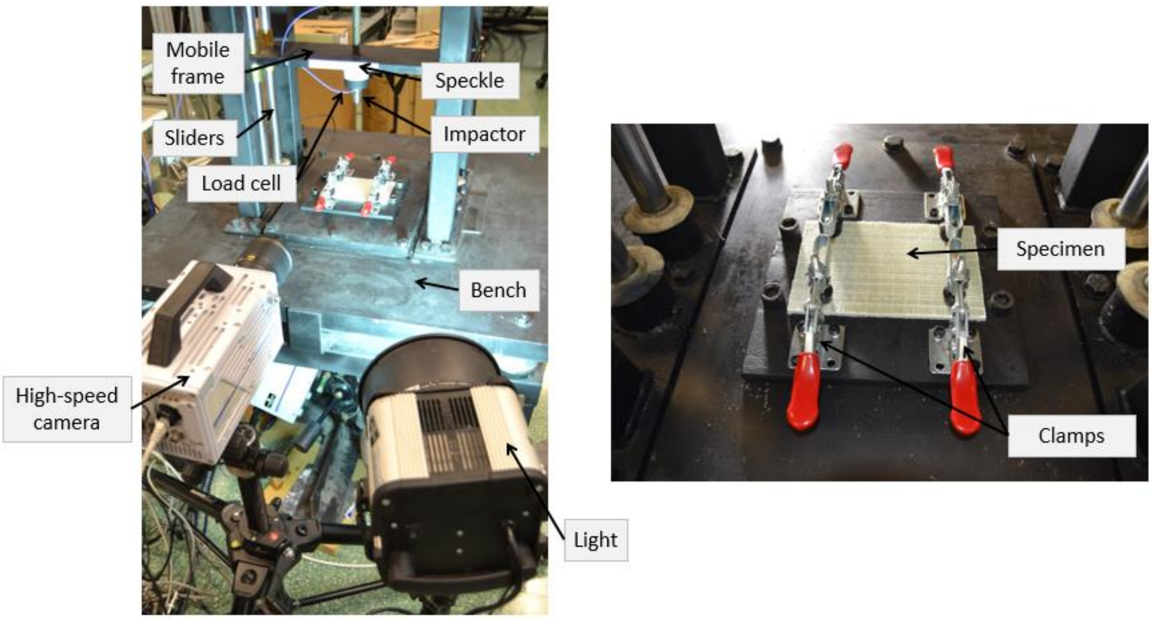

Figure 4. Set-up for impact tests, using a DIC system to measure the impactor position.

Then, the absorbed energy by the specimen was assessed using the Eq. 3~~Eq. 3~~, where E_a is the absorbed energy at time t, m is the mobile frame mass, v_i is the initial impactor velocity at the point of impact, $v(t)$ is the impactor velocity at time t, g is the acceleration due to gravity, and $\delta(t)$ is the impactor displacement at time t.

$$E_a = \frac{m \cdot (v_i^2 - v(t)^2)}{2} + m \cdot g \cdot \delta(t) \qquad \text{Eq. 3}$$

3. Results and discussion

3.1. Tensile tests

In the first experiment, different fibre orientations were impregnated without control system. The goal of this experiment was to evaluate the real impregnation velocity at the position where specimens were cut. As the specimens were distributed along the flow path, specimens manufactured at different velocities were collected. Also, the algorithm was tested for the different fiber arrangements and permeabilities. As expected, the flow-aligned (i.e. $[0_2]$) configuration shows the shortest impregnation time (34.0 s) and the highest impregnation velocities. Moreover, the cross-flow oriented configuration shows the lowest impregnation time (46.3 s) as well as the lowest impregnation velocities. The permeability values of each case are behind these differences. After manufacturing, the specimens were cut and tensile tests were performed.

Figure 5 shows the results of tensile test for the three different fiber orientations. Tensile modulus and tensile strength have been plotted as a function of the impregnation velocity. Although a high dispersion is observed in the experimental data, significate differences are reported when intermediate velocity values are compared with high and low values. Values have been adjusted by a straight line in the x-log plot, as also other authors did [19]. The highest values can be found in the range from 2 mm/s to 6 mm/s, where the three tested fiber orientations report their maximums. At 0º, the mean value of tensile strength in this range was 233 ± 46 MPa while the mean of all specimens was 191.4 ± 42.5 MPa, which means an increase of 21.7 %. Similarly, increases of 13.2% and 12.0% was measured at 45º and 90º, respectively. For tensile modulus, increases of 5.5%, 8.3% and 7.4% was measured for fibers at 0º, 45 and 90º, respectively. The less sensitive orientation was 0º since this case is the less sensitive to matrix properties, as highlighted in the revision of Mehdikhani et al. [16]. It should be highlighted that in all cases, tensile modulus and tensile strength are higher than the mean in the range of the considered optimum values. Indeed, the relative increase in strength is higher than the modulus. It can be explained when the voids in the material are considered as stress raisers. Since the volume of the microvoids and macrovoids is relatively small, the effect in the cross sectional area is limited and the modulus does not change noticeably. Nevertheless, the tensile stress at the voids surface is noticeably higher than the mean stress and the breakage is reached before the corresponding yield point without voids.

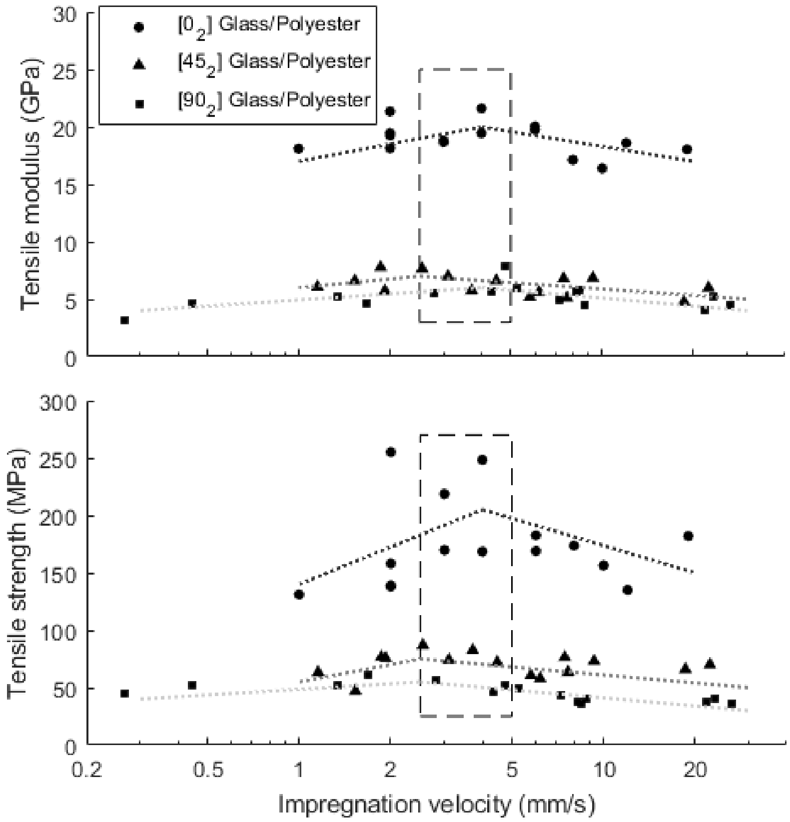

Figure 5. Tensile modulus (top) and strength (bottom) at different fibre orientations show intermediate optimum values.

3.2. Impact tests

Firstly, unstitched $[0_2,90]_S$ specimens were impacted at 13 ± 0.1 J, and after at 26 ± 0.2 J. The results are shown in Figure 6 where the two energies have been plotted once the signal filtering is applied to remove the random vibration noise. At 13 J, all results are very repetitive among all specimens impregnated at the same velocity, where the mean standard deviation is lower than 0.6%. The maximum values were obtained at 6.0 mm/s (3999 ± 16 N). The values in the range from 4 mm/s to 6 mm/s are only 1.9% higher than those out of this range (maximum of 3999 ± 16 N was obtained at 6.0 mm/s). At 26 J, the differences are more noticeable. The mean value in the range from 4 mm/s to 6 mm/s (dashed square) is 6499 ± 290 N, while the mean value out of this range was 5794 ± 526 N which represents an increase of 12.2%. These values are within the ranges shown by other authors, as reviewed by Mehdikhani et al. [16] for impact loads when voids are present.

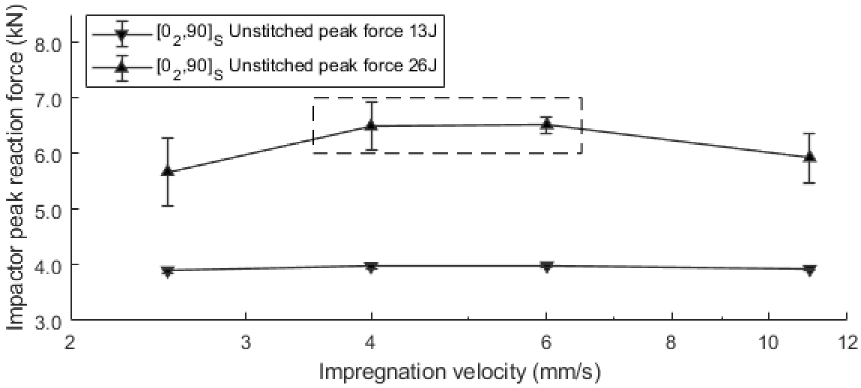

Figure 6. Impactor peak force at the tested flow front velocities for unstitched laminates. Specimens were impacted at 13 J and reimpacted at 26 J.

The same tests were performed with stitched and unstitched $[90_2,0]_S$ laminates. The maximum peak force at the impactor is shown in Figure 7 for the different impregnation velocities. Optimum values have been found in the range from 5 mm/s to 7.5 mm/s (dashed rectangle). According to the results of the optimum range, the increase in the impact force is 3.9 % and 3.1 % for impact at 26 J and 13 J respectively. In all cases, the effect of velocity optimization is more limited in the case of stitched laminates. In these cases, the effect of stitching masks the effect of the velocity optimization. Indeed, the increase associated to stitching, according to Figure 7 is 9.7% and 6.4%, which is much higher than the increase by the velocity optimization. Then, because of the intrinsic effect of stitching, the mechanical performance of the stitched laminates is higher than the unstitched ones, even when those have been impregnated at optimized velocities.

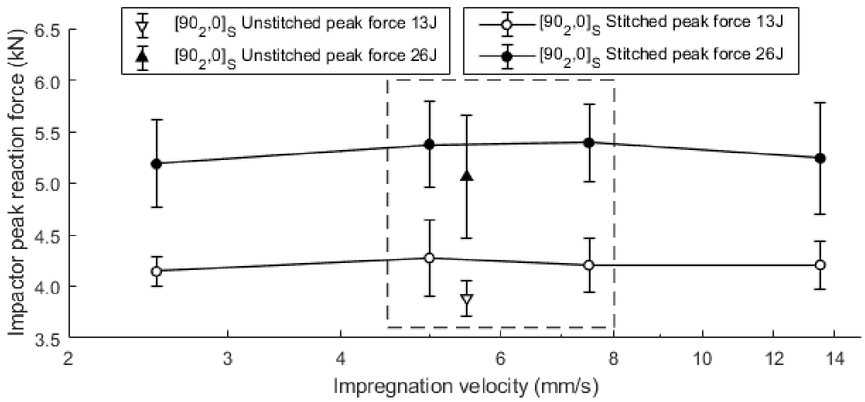

Figure 7. Impactor peak force at the tested flow front velocities for stitched and unstitched laminates, impacted at 13 J and reimpacted at 26 J.

The tracking of the impactor (Figure 8a) allows calculating the impactor position and velocity (Figure 8b), and the absorbed energy was evaluated (Figure 8c).

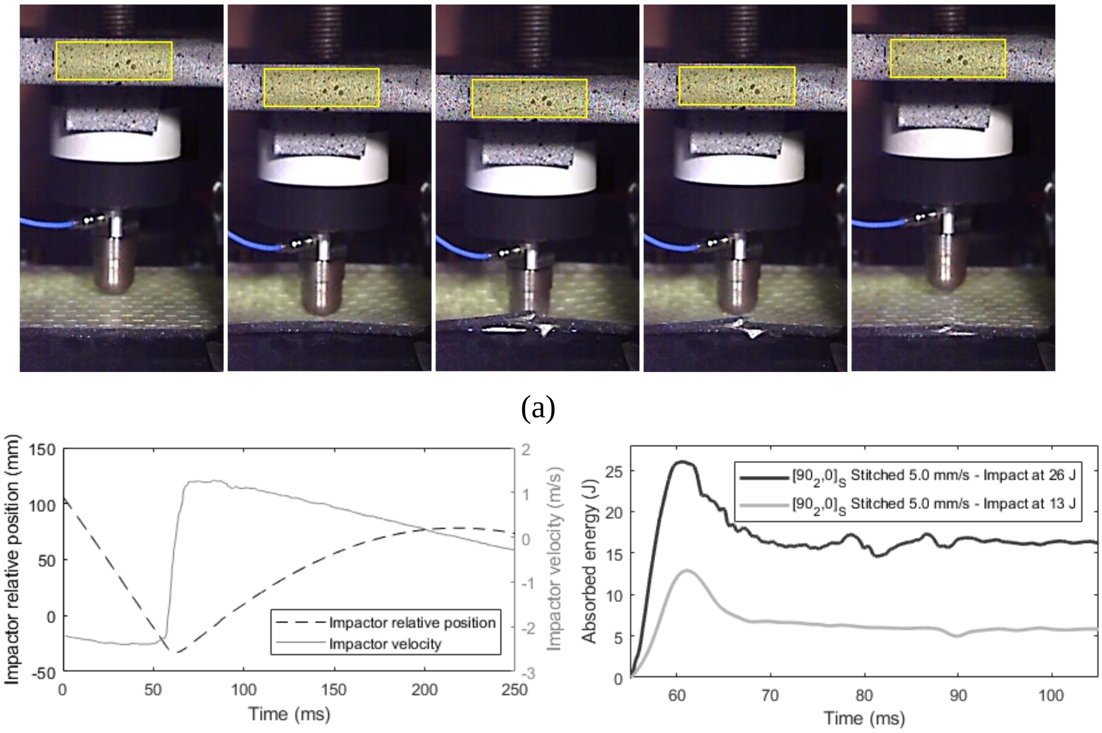

Figure 8. (a) Impactor position sequence, (b) impactor displacement and velocity data and (c) impactor dissipated energy during one impact event.

The absorbed energy in the specimens has been plotted in Figure 9~~Figure 9~~. As a result, no remarkable differences have been observed in the case of low energy impacts, where only the unstitched laminate and the stitched which was impregnated at the highest velocity shows a slight increment. Then, the stitching and the velocity optimization have a not very relevant effect at low energies. At 13 J, the measured energy was 6.4 J for the specimens manufactured at 2.5 mm/s, 5.0 mm/s and 7.5 mm/s, and 7.0 J for the specimen manufactured at 13.5 mm/s. Also, 7.5 J were measured in the case of unstitched laminate manufactured at 5.5 mm/s. It means that the optimized laminates show reductions up to 8.6 % of absorbed energy while adding stitching shows reductions up to 14.6%. On the other hand, at 26 J, higher differences are concluded. At 26 J, the measured energies were 18.8 J, 15.6 J, 17.9 J and 19.3 J for specimens manufactured at 2.5 mm/s, 5.0 mm/s, 7.5 mm/s and 13.5 mm/s respectively. Also, 20.6 J was measured for the specimen manufactured at 5.5 mm/s. It means that velocity optimization can decrease the absorbed energy up to 19.2% while adding stitching shows reductions up to 24.3%, as damaged area is smaller in both cases.

Summarizing, the unstitched laminates show the highest absorbed energy due to extended damage has been generated as delaminations. Specimens impacted at low energy have absorbed roughly the same energy. At high energy, the effect of optimized impregnation is remarkable, and the best results have been reported at 5 mm/s. The farther away from the optimum value, the higher absorbed energy in form of damage. This optimum value is slightly higher than the optimum values for tensile tests. Consequently, a more negative effect of macrovoids is reported for impact loads. It means that macrovoids and microvoids have a different impact on mechanical properties, as was also reported by [21].

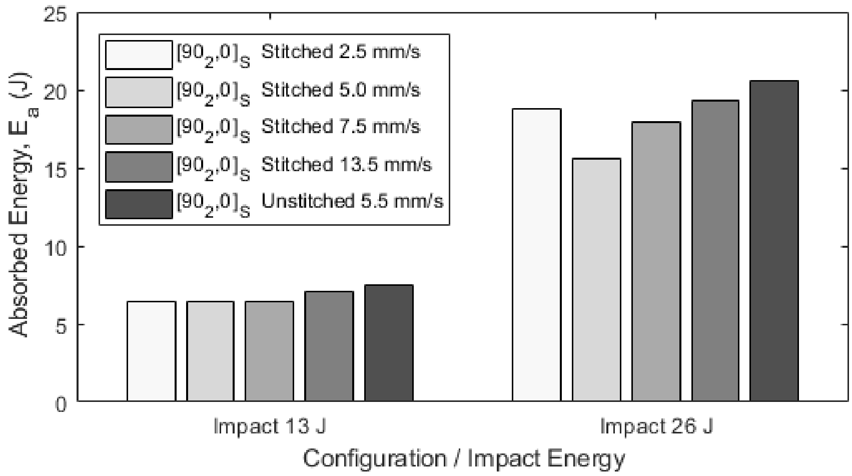

Figure 9. Absorbed energy in the range of analyzed velocities at the two energy levels, for stitched and unstitched laminates.

To explain these differences, the damage has been analyzed. Figure 10Figure 10 shows the backlight images of both types of specimens after 26 J re-impacts in which clearer areas mean highly damaged areas. Figure 10Figure 10a shows an unstitched laminate which was impregnated at high velocity. Figure 10Figure 10b shows the configuration impregnated at the optimum velocity, and damage has been clearly reduced and concentrated around the impact point. Figure 10Figure 10c shows a stitched configuration which was impregnated at high velocity while Figure 10Figure 10d corresponds to the optimized impregnation. When both unstitched are compared, the optimized one shows a more concentrated damage with shorter propagation distances. The same can be observed for the stitched laminates. When the unstitched and stitched are compared, it can be concluded that the stitching is very effective as it can limit the damage propagation. Once stitching is included, the damage is mainly propagated along the seam lines as stitches work as stress raises and cracks find the propagation easier along these weak points. Stitching is avoiding the extensive propagation of the delaminations. In the unstitched, instead, the damage is not restrained and large delaminated areas are observed. Then, stitching has modified the primary fracture mechanism from large interlaminar delaminations to crack propagation through the seams.

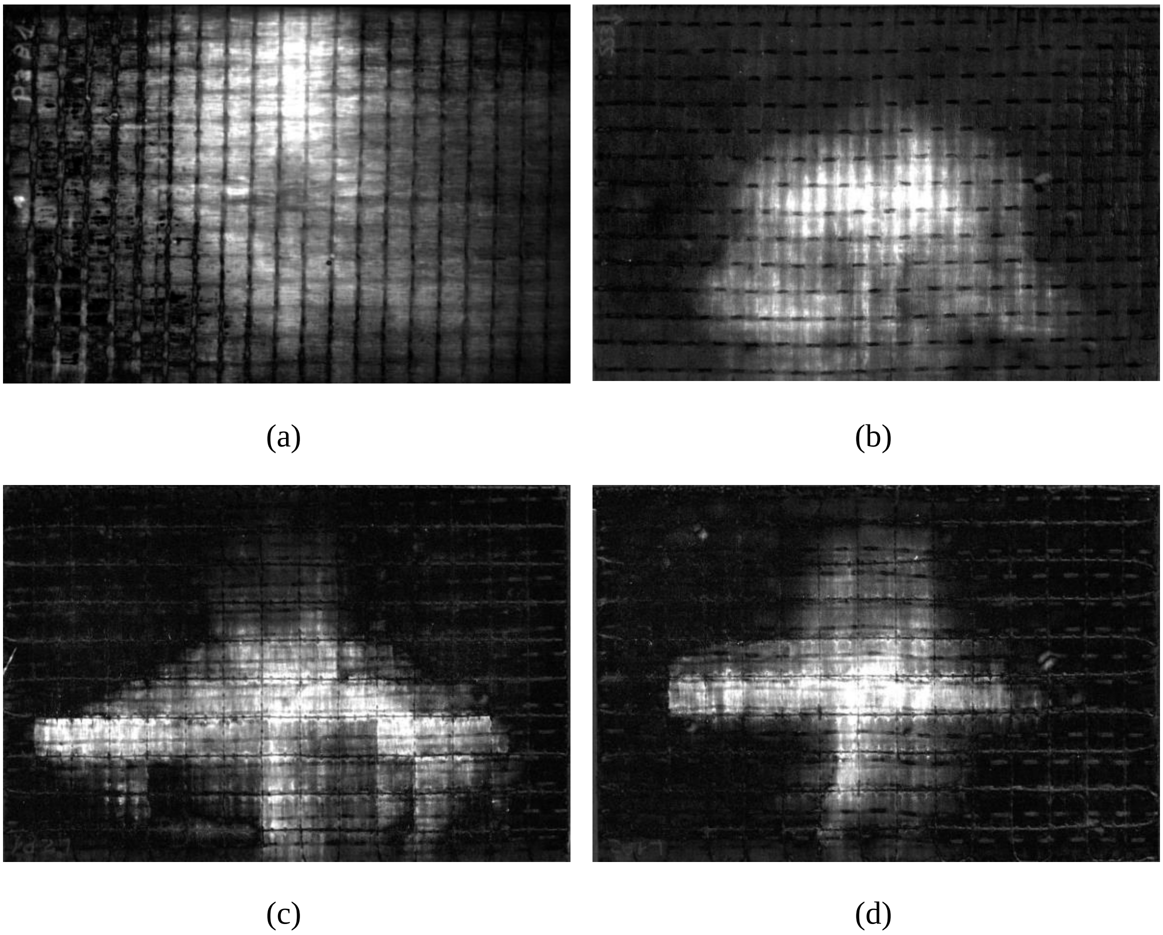

Figure 10. Damage backlight images of specimens after the 26 J re-impacts. (a) Unstitched and unoptimized, (b) unstitched and optimized; (c) stitched unoptimized and (d) stitched and optimized.

The effect of stitching can also be noticed when a cross-sectional view at the damaged area is analyzed. Figure 11~~Figure 11~~ shows a comparative images of unstitched and stitched laminates after being impacted. Extended delaminations have been observed in the unstitched laminates (Figure 11~~Figure 11~~a), where no links are present to keep consecutive plies together when shear stress is generated at the interface. It promotes large delaminations through the interfaces. On the other hand, stitching has avoided the delamination from be extensively propagated (Figure 11~~Figure 11~~b). Nevertheless, large voids (i.e. macrovoids) have been observed near the stitching points as a consequence of the yarn distortions because of the transversal stitches. In both cases, macrovoids have been observed in the internal plies. As a result, stitching changes the damage mechanism for impact loads as delaminations are avoided while crack propagation through the seams are promoted. Despite of these two opposite effects of stitching, taking into account the mechanical results of impact force and absorbed energy, the impact behaviour has been enhanced by using stitching.

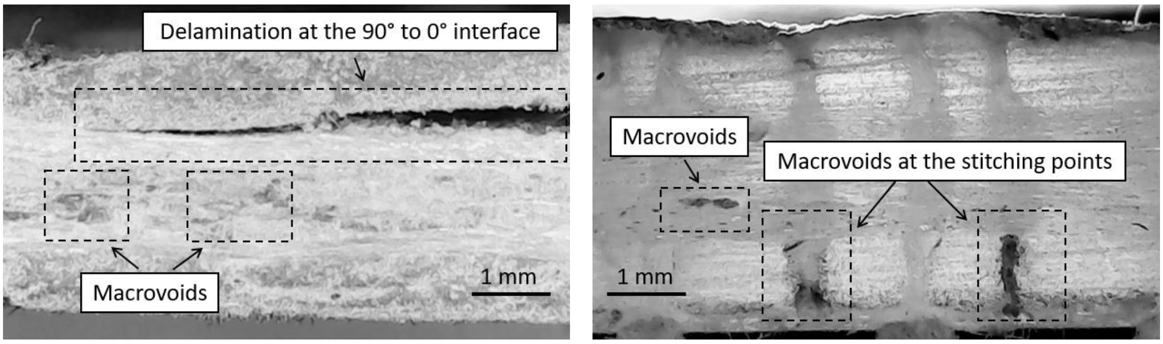

(a) (b)

Figure 11. Cross sectional views after 26 J impacts. (a) Unstitched laminate, where large delaminations have been observed; and (b) stitched laminate where delaminations have been avoided by the stitching linking effects, although macrovoids are shown near the stitching points at the mold face.

5. Conclusions

In this work, the application of control system in composites manufacturing has been successfully applied in the RI process. The tensile and impact properties have been improved in unstitched and stitched laminates.

Both tensile and impact tests have reported optimum impregnation velocities in the range from 2.5 mm/s to 8.0 mm/s. In this range, slightly higher values have been observed in the case of impact properties, that means that the mechanical effect of microvoids and macrovoids are different within the type of load. Non-significant differences have been observed in the optimum flow front velocity as a function of the fibre orientation. Further experimental tests may clarify this relation.

The application of the flow front controller is highly effective for high energy impacts, while only slight improvements have been reported at low energy impacts. Similarly, stitching is specifically effective at high-energy impacts, where the extension of the delaminations are restrained and limited. The impregnation velocity in stitched laminates can also be optimized. Similar ranges for the optimums have been reported. It means that the presented methodology can be successfully used in complex laminates manufacturing by RI.

Acknowledgments

Authors gratefully acknowledge to the Leibniz Institute for Composite Materials (Kaiserslautern, Germany).

This work was supported by Airbus Defence and Space in the Apolo “*Alas de turbopropulsor mediante optimización logística y desarrollo online*” project.

References

[1] Khan, L. A. and A. H. Mehmood, ‘5 - Cost-effective composites manufacturing processes for automotive applications’, J. B. T.-L. C. S. in T. Njuguna, Ed. Woodhead Publishing, 2016, pp. 93–119.

[2] Mallick, P. K., *Materials, Design and Manufacturing for Lightweight Vehicles*. Woodhead Publishing, 2010.

[3] Sterk, S. and H. P. J. Vries, ‘Low Cost Automated Manufacturing of an A320 Slat Fairing’, in *Proc. of SAMPE Europe SEICO 2014 - 35th Int. Technical Conf. & Forum*, 2014.

[4] Björnsson, A., M. Jonsson, and K. Johansen, ‘Automated material handling in composite manufacturing using pick-and-place systems – a review’, *Robot. Comput. Integr. Manuf.*, vol. 51, pp. 222–229, 2018, doi: https://doi.org/10.1016/j.rcim.2017.12.003.

[5] Willicombe, K. G., M. P. Elkington, I. Hamerton, and C. Ward, ‘Development of Novel Transportation Shells for the Rapid, Automated Manufacture of Automotive Composite Parts ’, *Procedia Manufacturing* , vol. 51. pp. 818–825, Nov. 19, 2020, doi: 10.1016/j.promfg.2020.10.115.

[6] Budwal, N., K. Kasper, J. Goering, and C. Ward, ‘Flexible low-cost tooling solutions for a one-shot resin infusion of a 3D woven and multi-textile preform’, *Procedia Manuf.*, vol. 51, pp. 856–863, 2020, doi: https://doi.org/10.1016/j.promfg.2020.10.120.

[7] Gerngross, T. and D. Nieberl, ‘Automated manufacturing of large, three-dimensional CFRP parts from dry textiles’, *CEAS Aeronaut. J.*, vol. 7, no. 2, pp. 241–257, 2016, doi: 10.1007/s13272-016-0184-5.

[8] Carlone, P., L. Sorrentino, and R. M. Kent, ‘7.16 Process Control for Polymeric Composite Manufacture’, P. W. R. Beaumont and C. H. B. T.-C. C. M. I. I. Zweben, Eds. Oxford: Elsevier, 2018, pp. 337–354.

[9] Alms, J. B., S. G. Advani, and J. L. Glancey, ‘Liquid Composite Molding control methodologies using Vacuum Induced Preform Relaxation’, *Compos. Part A Appl. Sci. Manuf.*, vol. 42, no. 1, pp. 57–65, 2011, doi: https://doi.org/10.1016/j.compositesa.2010.10.002.

[10] Sozer, E. M., S. Bickerton, and S. G. Advani, ‘On-line strategic control of liquid composite mould filling process’, *Compos. Part A Appl. Sci. Manuf.*, vol. 31, no. 12, pp. 1383–1394, 2000, doi: https://doi.org/10.1016/S1359-835X(00)00060-9.

[11] Devillard, M., K.-T. Hsiao, and S. G. Advani, ‘Flow sensing and control strategies to address race-tracking disturbances in resin transfer molding—part II: automation and

validation', *Compos. Part A Appl. Sci. Manuf.*, vol. 36, no. 11, pp. 1581–1589, 2005, doi: https://doi.org/10.1016/j.compositesa.2004.04.009.

[12] Seyednourani, M., M. Yildiz, and H. S. Sas, 'A two-stage optimization methodology for gate and vent locations and distribution media layout for liquid composite molding process', *Compos. Part A Appl. Sci. Manuf.*, vol. 149, p. 106522, 2021, doi: https://doi.org/10.1016/j.compositesa.2021.106522.

[13] Rajak, D. K., D. D. Pagar, P. L. Menezes, and E. Linul, 'Fiber-Reinforced Polymer Composites: Manufacturing, Properties, and Applications', *Polymers* , vol. 11, no. 10. 2019, doi: 10.3390/polym11101667.

[14] Darcy, H., 'Les fontaines publiques de la ville de Dijon: exposition et application', *Dalmont*, p. 647, 1856, doi: 10.1080/00150199208223391.

[15] Ruiz, E., V. Achim, S. Soukane, F. Trochu, and J. Bréard, 'Optimization of injection flow rate to minimize micro/macro-voids formation in resin transfer molded composites', *Compos. Sci. Technol.*, vol. 66, no. 3–4, pp. 475–486, 2006, doi: 10.1016/j.compscitech.2005.06.013.

[16] Mehdikhani, M., L. Gorbatikh, I. Verpoest, and S. V Lomov, 'Voids in fiber-reinforced polymer composites: A review on their formation, characteristics, and effects on mechanical performance', *J. Compos. Mater.*, vol. 53, no. 12, pp. 1579–1669, Nov. 2018, doi: 10.1177/0021998318772152.

[17] Caglar, B., C. Tekin, F. Karasu, and V. Michaud, 'Assessment of capillary phenomena in liquid composite molding', *Compos. Part A Appl. Sci. Manuf.*, vol. 120, pp. 73–83, 2019, doi: https://doi.org/10.1016/j.compositesa.2019.02.018.

[18] Michaud, V., 'A Review of Non-saturated Resin Flow in Liquid Composite Moulding processes', *Transp. Porous Media*, vol. 115, no. 3, pp. 581–601, 2016, doi: 10.1007/s11242-016-0629-7.

[19] Causse, P., C. Ravey, and F. Trochu, 'Capillary Characterization of Fibrous Reinforcement and Optimization of Injection Strategy in Resin Transfer Molding', *Journal of Composites Science* , vol. 2, no. 2. 2018, doi: 10.3390/jcs2020019.

[20] Ashir, M., A. Nocke, A. Bulavinov, R. Pinchuk, and C. Cherif, 'Influence of defined amount of voids on the mechanical properties of carbon fiber-reinforced plastics', *Polym. Compos.*, vol. 40, no. S2, pp. E1049–E1056, 2019, doi: 10.1002/pc.24820.

[21] Leclerc, J. S. and E. Ruiz, 'Porosity reduction using optimized flow velocity in Resin Transfer Molding', *Compos. Part A Appl. Sci. Manuf.*, vol. 39, no. 12, pp. 1859–1868, 2008, doi: 10.1016/j.compositesa.2008.09.008.

[22] Olivero, K. A., H. J. Barraza, E. A. O'Rear, and A. M. C., 'Effect of Injection Rate and Post-Fill Cure Pressure on Properties of Resin ransfer Molded Disks', *J. Compos. Mater.*, vol. 36, pp. 2011–2028, 2002, doi: 10.1177/0021998302036016244.

[23] Patou, J., G. Bernhart, and E. De Luycker, ‘Influence of void content on the mechanical properties of carbon / PPS laminates’, in *ECCM17 - 17th European Conference on Composite Materials*, Jun. 2016.

[24] Kopparthi, P., V. Kundavarapu, V. Dasari, and B. Pathakokila, ‘Determination of flow front velocity and optimal injection pressures for better impregnation of E-glass with polyester in resin transfer mold’, *Incas Bull.*, vol. 11, pp. 87–98, 2019, doi: 10.13111/2066-8201.2019.11.3.8.

[25] Trochu, F., E. Ruiz, V. Achim, and S. Soukane, ‘Advanced numerical simulation of liquid composite molding for process analysis and optimization’, *Compos. Part A Appl. Sci. Manuf.*, vol. 37, no. 6, pp. 890–902, 2006, doi: https://doi.org/10.1016/j.compositesa.2005.06.003.

[26] He, P., W. Zhao, B. Yang, J. Wang, A. Ni, and S. Li, ‘Void content reduction of composites with sensor-aided injection strategy in liquid composite molding process’, *Mater. Res. Express*, vol. 8, no. 7, 2021, doi: 10.1088/2053-1591/ac1532.

[27] Fratta, C. Di, G. Koutsoukis, F. Klunker, and P. Ermanni, ‘Fast method to monitor the flow front and control injection parameters in resin transfer molding using pressure sensors’, *J. Compos. Mater.*, vol. 50, no. 21, pp. 2941–2957, 2016, doi: 10.1177/0021998315614994.

[28] Endruweit, A., P. McGregor, A. C. Long, and M. S. Johnson, ‘Influence of the fabric architecture on the variations in experimentally determined in-plane permeability values’, *Compos. Sci. Technol.*, vol. 66, no. 11, pp. 1778–1792, 2006, doi: https://doi.org/10.1016/j.compscitech.2005.10.031.

[29] Ahn, S. H., W. Il Lee, and G. S. Springer, ‘Measurement of the Three-Dimensional Permeability of Fiber Preforms Using Embedded Fiber Optic Sensors’, *J. Compos. Mater.*, vol. 29, no. 6, pp. 714–733, Apr. 1995, doi: 10.1177/002199839502900602.

[30] Grössing, H. *et al.*, ‘An evaluation of the reproducibility of capacitive sensor based in-plane permeability measurements: A benchmarking study’, *Express Polym. Lett.*, vol. 9, no. 2, pp. 129–142, Feb. 2015, doi: 10.3144/expresspolymlett.2015.14.

[31] Geng, Y., J. Jiang, F. Lin, H. Shao, C. Zhang, and N. Chen, ‘Study of Compaction Properties and Permeability Prediction of Multilayered Quadriaxial Non-Crimp Fabric in Liquid Composite Molding Process’, *Polymers* , vol. 12, no. 7. 2020, doi: 10.3390/polym12071525.

[32] Vernet, N. *et al.*, ‘Experimental determination of the permeability of engineering textiles: benchmark II’, *Compos. A*, vol. 61, pp. 172–184, 2014, doi: 10.1016/j.compositesa.2014.02.010.

[33] Rieber, G. and P. Mitschang, ‘2D Permeability changes due to stitching seams’, *Compos. Part A Appl. Sci. Manuf.*, vol. 41, no. 1, pp. 2–7, 2010, doi:

10.1016/j.compositesa.2009.09.006.

[34] Kumar, B. and S. Thakur, *Textiles for Advanced Applications*. London, UK: InterchOpen, 2017.

[35] Gnaba, I., X. Legrand, P. Wang, and D. Soulat, 'Through-the-thickness reinforcement for composite structures: A review', *J. Ind. Text.*, vol. 49, no. 1, pp. 71–96, Apr. 2018, doi: 10.1177/1528083718772299.

[36] Kumari, P., J. Wang, and Saahil, 'Residual Tensile Strength of the Multi-Impacted Scarf-Repaired Glass Fiber-Reinforced Polymer (GFRP) Composites', *Materials (Basel).*, vol. 11, p. 2351, 2018, doi: 10.3390/ma11122351.

[37] ASTM International, *ASTM D3039 - Standard Test Method for Tensile Properties of Polymer Matrix Composite Materials*. 1995.

[38] ASTM International, 'ASTM D7136/D7136M. Standard Test Method for Measuring the Damage Resistance of a Fiber-Reinforced Polymer Matrix Composite to a Drop-Weight Impact Event', 2012. doi: 10.1520/D7136.